Chemistry–A European Journal
Research Article
doi.org/10.1002/chem.202304097
Chemistry Europe
European Chemical Societies Publishing
www.chemeurj.org

Direct Band Gap Semiconductors with Two- and Three-Dimensional Triel-Phosphide Frameworks (Triel=Al, Ga, In)

Tassilo M. F. Restle[+],[a] Sabine Zeitz[+],[a] Philip M. Stanley[+],[b] Antti J. Karttunen[+],[c] Jan Meyer[+],[a] Gabriele Raudaschl-Sieber[+],[b] Wilhelm Klein[+],[a] and Thomas F. Fässler[+*][a]

Recently, several ternary phosphidotrielates and -tetrelates have been investigated with respect to their very good ionic conductivity, while less focus was pointed towards their electronic structures. Here, we report on a novel series of compounds, in which several members possess direct band gaps. We investigated the known compounds Li_3AlP_2, Li_3GaP_2, Li_3InP_2, and Na_3InP_2 and describe the synthesis and the crystal structure of novel $Na_3In_2P_3$. For all mentioned phosphidotrielates reflectance UV-Vis measurements reveal direct band gaps in the visible light region with decreasing band gaps in the series: Li_3AlP_2 (2.45 eV), Li_3GaP_2 (2.18 eV), Li_3InP_2 (1.99 eV), Na_3InP_2 (1.37 eV), and $Na_3In_2P_3$ (1.27 eV). All direct band gaps are confirmed by quantum chemical calculations. The unexpected property occurs despite different structure types. As a common feature all compounds contain EP_4 tetrahedra, which share exclusively vertices for *E*=In and vertices as well as edges for *E*=Al and Ga. The structure of the novel $Na_3In_2P_3$ is built up by a polyanionic framework of six-membered rings of corner-sharing InP_4 tetrahedra. As a result, the newly designed semiconductors with direct band gaps are suitable for optoelectronic applications, and they can provide significant guidance for the design of new functional semiconductors.

Introduction

Direct band gap semiconductors show a much higher efficiency in optoelectronic applications and thus the search for new compounds with direct band gaps is a big challenge. Newly designed and experimentally realized semiconductors with direct band gaps are rare, and therefore representatives that provide significant guidance for the design of new functional semiconductors are indispensable. The recently discovered ternary alkali-metal pnictides of triel and tetrel elements have attracted considerable attention with respect to rechargeable lithium- and sodium-ion batteries, while less focus was pointed towards their electronic structures. Layered tetrel pnictides GeP, Sn_4P_3, SiAs, GeAs, and SiP_2 have been investigated as active material for lithium- and sodium-ion batteries,[1–6] and efforts of our group have led to the discovery of a new class of ion conductors in the series of lithium-rich phosphidotrielates and tetrelates. Li_8TtP_4 (*Tt*=Si, Ge, Sn) are good ion conductors in the range between 0.6 and 6.6×10^{-4} S cm^{-1}, Li_9TrP_4 (Tr=Al, Ga) shows superionic conducting behavior with lithium ionic conductivities of up to 3×10^{-3} S cm^{-1} at room temperature.[7–12] The ternary phases comprise discrete $[TtP_4]^{8-}$ and $[TrP_4]^{9-}$ tetrahedra, which are surrounded by lithium atoms. At lower lithium content, the EP_4 tetrahedra are condensed *via* vertex- or edge-sharing tetrahedra into two-dimensional networks (2D) such as in $Li_3Si_3P_7$, $LiGe_3P_3$, Li_3AlP_2, and Li_3GaP_2 as well as three-dimensional networks (3D) found in Li_2SiP_2, Li_2GeP_2, $LiSi_2P_3$, and Li_3InP_2.[13–18]

Compounds with linked triel pnictide tetrahedra such as in GaAs are among the most important 13–15 semiconductors,[19] and thus they are also important materials for the development of electronic devices e.g. in transistors or in light-emitting diodes on which our modern information age is based.[20–21] However, many of the known semiconductors like elemental silicon show only indirect band gaps leading to a much lower efficiency in optoelectronic applications, whereas InP, InAs, InSb, GaAs, and GaSb are direct band gap semiconductors.[19] These materials have received considerable attention in the last decades, since they have the potential as base materials for light-emitting diodes, infrared detectors, quantum dots, and quantum-well applications.[22–24] This drives efforts to synthesize new compounds, which may exhibit direct band gaps. In recent times, chalcogen-based materials like sulfides (e.g. SnS, PbS, ZnS, or $LiPbSb_3S_6$)[25–28] and selenides (e.g. ZnSe, $AAsSe_2$ with *A*=Li, Na)[28–30] as well as ternary alkaline earth arsenidosilicates such as $MgSiAs_2$ and $Mg_3Si_6As_8$[31] or phosphidosilicates (e.g. $Ba_2Si_3P_6$, Ba_2SiP_4)[32–33] gained attention as semiconductors, which in some cases possess direct or pseudo-direct band gaps, whereas transition metal phosphidosilicates $MnSiP_2$ or $RuSi_4P_4$ have indirect band gaps.[34–35]

[a] T. M. F. Restle,[+] S. Zeitz,[+] J. Meyer,[+] W. Klein,[+] Prof. Dr. T. F. Fässler[+]
Department of Chemistry, Chair of Inorganic Chemistry with Focus on New Materials, Technische Universität München, Lichtenbergstraße 4, D-85747 Garching, Germany
E-mail: Thomas.Faessler@lrz.tum.de

[b] P. M. Stanley,[+] G. Raudaschl-Sieber[+]
Department of Chemistry, Chair of Inorganic and Metal-Organic Chemistry, Technische Universität München, Lichtenbergstraße 4, D-85747 Garching, Germany

[c] A. J. Karttunen[+]
Department of Chemistry and Materials Science, Aalto University, FI-00076 Aalto, Finland

[+] The authors declare no competing financial interest

Supporting information for this article is available on the WWW under https://doi.org/10.1002/chem.202304097

Based on Density Functional Theory (DFT) calculations, Li_3AlP_2 and Li_3GaP_2 were reported as semiconductors with direct band gaps of 3.1 eV and 2.8 eV, respectively.[15] Due to these promising clues, we focused now on the systematic search for phosphide-based materials with optical properties, and establish here the series Li_3AlP_2, Li_3GaP_2, Li_3InP_2, Na_3InP_2,[36] and $Na_3In_2P_3$ as direct band gap semiconductors.

Results and Discussion

Syntheses

The compounds Li_3AlP_2, Li_3GaP_2 and Li_3InP_2 were synthesized according to literature *via* ball milling and subsequent annealing at 1023 K.[15,18] Li_3AlP_2 appears as single-phase material, Li_3GaP_2 and Li_3InP_2 contain very small amounts of GaP and $Li_{0.3}In_{1.7}$, respectively, as side phase (Figure S6). Na_3InP_2 was synthesized *via* the ball milling approach. Subsequent annealing of the ball-milled mixture at 673 K led to almost phase-pure Na_3InP_2, with only a few unknown reflections with low intensity (Figure S4).

The element ratio of the new compound $Na_3In_2P_3$ was chosen according to the Gibbs composition triangle on the line between the binary compositions Na_3P and InP (Figure S1). $Na_3In_2P_3$ was also synthesized from the elements *via* a two-step procedure including ball milling of the elements in a stoichiometric ratio and a subsequent annealing step. $Na_3In_2P_3$ contains only very small amounts of impurities (according to the Rietveld refinement in Figure 1 approximately 2% Na_3InP_2 and 1% InP, Tables S1 and S2). $Na_3In_2P_3$ was further characterized by DSC (Figure S8 and S9) and ^{31}P NMR spectroscopy (Figure S10). Impedance spectroscopy does not indicate any ionic conductivity and only very poor electronic conductivity. All details can be found as Supporting Information (Figure S11–S12).

Crystal Structures of Li_3AlP_2, Li_3GaP_2, Li_3InP_2, and Na_3InP_2

A common structural feature of Li_3AlP_2, Li_3GaP_2, Li_3InP_2, and Na_3InP_2 are TrP_4 units that build the anionic substructure. Li_3AlP_2 and Li_3GaP_2 exhibit a two-dimensional polyanionic framework consisting of edge-sharing Tr_2P_6 dimers which are corner-connected to give layers (Figure 2a).[15] Li_3InP_2 contains InP_4 tetrahedra which are connected *via* corners to T2-supertetrahedra.[18] These T2-supertetrahedra share vertices and form a three-dimensional framework. Two of such independent adamantane-like networks, which are emphasized in Figure 2b by the colors red and blue, are interpenetrating. Na_3InP_2 is built up by InP_4 units, which form a three-dimensional polyanionic framework of corner- and edge-sharing tetrahedra (Figure 2c).[36]

As expected the *Tr*–*Tr* distances are shorter for the compounds with edge-sharing connectivity of the tetrahedra (Table 1). The occurrence of edge-sharing tetrahedra is accompanied by a higher distortion of the tetrahedra, which is reflected in a wider range of P–*Tr*–P angles. The *Tr*–P distances increase with increasing triel ionic radius.

Crystal Structure of $Na_3In_2P_3$

Grey single crystals of $Na_3In_2P_3$ were obtained by the reaction of the elements with excess of In and P corresponding to a formal stoichiometry of "$Na_3In_4P_5$" at 1073 K in tantalum ampoules. The details of the structure refinement of $Na_3In_2P_3$ from single crystal X-ray diffraction (SC-XRD) data are listed in Table S3. $Na_3In_2P_3$ crystallizes in the orthorhombic space group $Cmc2_1$

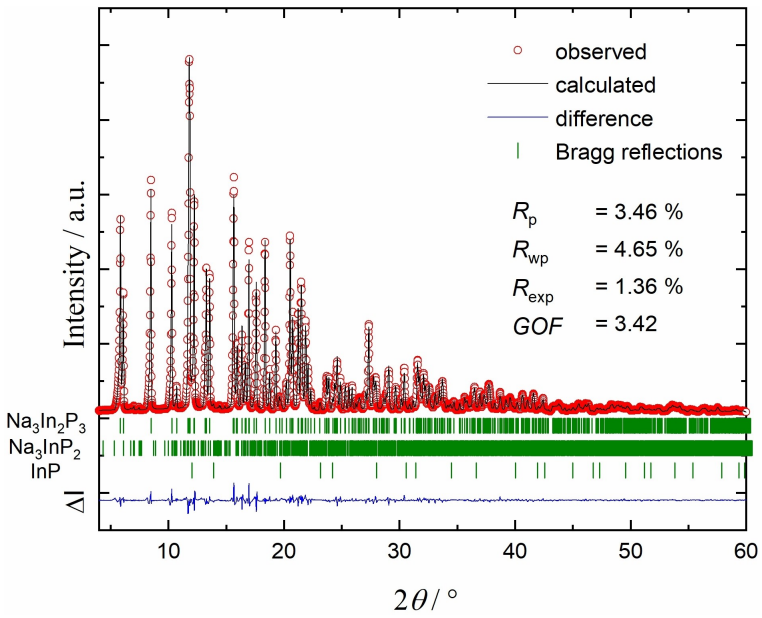

Figure 1. Rietveld analysis of the powder X-ray diffractogram of $Na_3In_2P_3$. The red line indicates the observed intensities, the black line the calculated intensities and the blue line the difference between both. Bragg positions are marked by green dashes. The $Na_3In_2P_3$:Na_3InP_2:InP ratio is 97.0(1):1.8(1):1.2(1) wt.-%.

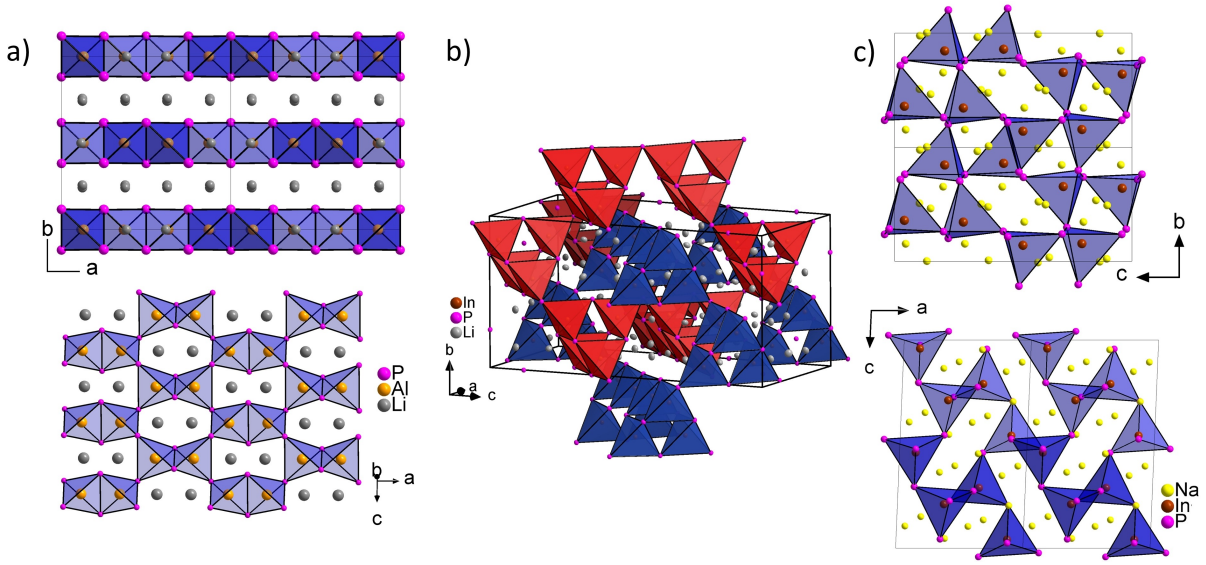

Figure 2. Comparison of the structures of a) Li_3AlP_2 and Li_3GaP_2,[15] b) Li_3InP_2[18] and c) Na_3InP_2.[36] a) Li_3AlP_2 and Li_3GaP_2 show a two-dimensional layer structure of corner- and edge-sharing TrP_4 tetrahedra; b) Li_3InP_2 displays a three-dimensional network of T2 supertetrahedra built up by exclusively corner-sharing InP_4 tetrahedra; c) Na_3InP_2 contains a three-dimensional network of corner- and edge-sharing InP_4 tetrahedra. TrP_4 tetrahedra are highlighted in blue or red. The Li, Na, Al, In, and P atoms are drawn in grey, yellow, orange, brown, and purple, respectively.

(no. 36) with five independent crystallographic positions (In, P1, P2, Na1, Na2) (Table S4). $Na_3In_2P_3$ (Figure 3) contains a polyanionic framework of exclusively corner-sharing InP_4 tetrahedra, which are surrounded by Na^+ ions. These InP_4 tetrahedra are connected in the *a*/*b* plane to form layers of six-membered rings (see Figures 3a, S15a). This type of layer structure of six-membered rings is known from layered silicates like sepiolite, $A_xB_ySi_zO_a$ (for a comparison see Figure S15b).[37] With respect to the centre of the tetrahedra (In atoms), the layers of the six-membered rings can be considered as a hierarchical variant of the graphite-type network parallel to the *a*/*b* plane (Figure 3d), however, the layers are three-dimensionally connected in the *c* direction (Figure 3b). Each indium atom is surrounded by four phosphorus atoms, while phosphorus is located at two crystallographic sites with different connectivities to the indium atoms: P1 has two indium neighbors, whereas P2 has three and thus is part of three InP_4 tetrahedra (Figure 3a and b). All tetrahedra of one graphite-like layer are oriented in such a way that one tetrahedral face is perfectly parallel to the *ab* plane, and all opposing faces point upward. As a result, the graphite-type layers are shifted with respect to each other, as demonstrated in Figure 3d.

Alternatively, the structure of $Na_3In_2P_3$ can be described as a distorted hexagonal close packing (*hcp*) of phosphorus atoms with 24 tetrahedral and 12 octahedral voids with respect to 12 P atoms according the multiplicity of the Wyckoff positions $4a+8b$ of the phosphorus atoms. The *hcp* of P atoms is emphasized in Figure 3c by *ABAB* layers of face-sharing NaP_6 octahedra. One third of the tetrahedral voids is filled by the indium atoms (Wyckoff position 8*b*), and the sodium atoms occupy all octahedral voids (Na1 with Wyckoff position 4*a* and Na2 with Wyckoff position 8*b*). As shown in Figure S14, all Na coordination octahedra are strongly distorted.

The In-P bond lengths in the InP_4 tetrahedra are in the range between 2.5704(7) and 2.6065(8) Å (Figure S13) and are thus very similar to those in known compounds with edge-sharing InP_4 tetrahedra, like Na_3InP_2 (2.592–2.682 Å),[36] Ca_3InP_3 (2.5616–2.6073 Å),[42] $Sr_3In_2P_4$ (2.5628–2.6467 Å),[43] and $Ba_3In_2P_4$ (2.5687–2.6463 Å),[44] or with corner-sharing tetrahedra, like Sr_3InP_3 (2.5628–2.6467 Å).[45] The average In-P bond lengths in $Na_3In_2P_3$ are shorter than in compounds with isolated InP_4 tetrahedra like $Ba_{14}InP_{11}$ (2.7134 Å),[46] but longer than in compounds, in which both atom types are tetrahedrally coordinated like in InP (2.5412 Å) with ZnS structure.[47] As

Table 1. Comparison of the *Tr*-P distances *d*(*Tr*-P), the P–*Tr*–P angles P–*Tr*–P and the *Tr*–*Tr* distances *d*(*Tr*–*Tr*) in Li_3AlP_2, Li_3GaP_2,[15] Li_3InP_2,[18] Na_3InP_2,[36] and $Na_3In_2P_3$.

	Li_3AlP_2	Li_3GaP_2	Li_3InP_2	Na_3InP_2	$Na_3In_2P_3$
d(*Tr*–P)/Å	2.398(3) −2.410(3)	2.404(2) −2.419(2)	2.5676(5) −2.5899(5)	2.592(4) −2.682(3)	2.5704(7) −2.6065(8)
(*P*–*Tr*–*P*)/°	101.70(1) −111.57(1)	100.6(1) −112.18(1)	107.20(1) −111.55(1)	100.2(1) −117.8(1)	100.56(2) −115.16(2)
d(*Tr*–*Tr*)/Å	3.0228(5) −3.989(3)	3.089(2) −3.969(1)	4.1122(3) −4.2793(5)	3.360(2) −4.784(4)	4.0782(3) −4.5691(5)

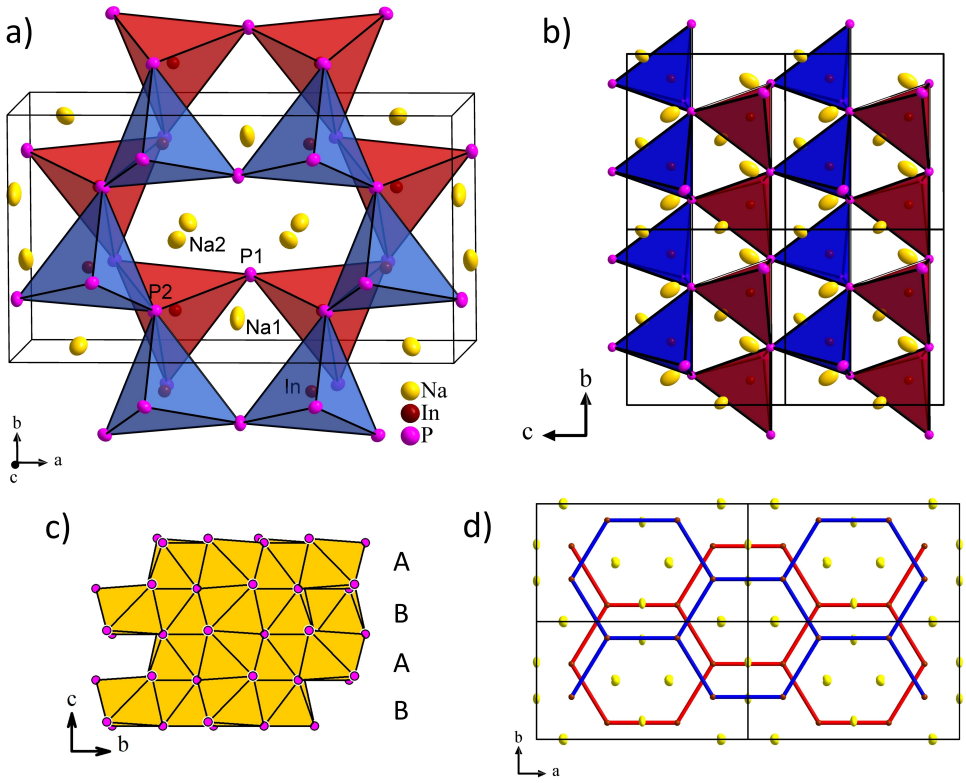

Figure 3. The crystal structure of $Na_3In_2P_3$. a) Extended unit cell with view in *c* direction. The InP_4 tetrahedra arranged in layers of six-membered rings in the *a*/*b* plane are shown in blue and red; b) 1×2×2 unit cells, view along [100]. The different InP_4 layers of six-membered rings are drawn in blue and red. The layers are connected to each other *via* P2; c) *ABAB* layers of face-sharing NaP_6 octahedra, illustrating the *hcp* of the phosphorus atoms; d) the In atoms form graphite-like layers parallel to the *a*/*b* plane. The Na, In and P atoms are drawn in yellow, brown and purple, respectively. The displacement ellipsoids are shown at a 90% probability level.

mentioned above, the InP_4 tetrahedra in $Na_3In_2P_3$ are connected to neighboring tetrahedra *via* all four corners, where one P atom (P1) is part of two and the remaining three (P2) are connecting even three tetrahedra. The distortion of the InP_4 tetrahedra as a result of these different connectivities is reflected by the deviation of the P–In-P angles between 100.56(2)° and 115.16(2)° from the ideal tetrahedral angle of 109.47°. The In–In distances (4.0782(3)–4.5691(5) Å) are in the same range as in Li_3InP_2 and are longer than in Na_3InP_2, which also contains edge-sharing tetrahedra (Table 1)[18,36] The Na–P bond lengths in $Na_3In_2P_3$ range from 2.818(2) to 2.990(4) Å. Overall, these distances are in good agreement with those in Na_3P[48] or in other ternary phases containing Na and P, such as Na_3AlP_2 and Na_3InP_2.[36,49]

Comparison of $Na_3In_2P_2$ with the structures of $NaSi_2N_3$, $LiSi_2N_3$, Si_2N_2NH, and Si_2N_2O

The polyanionic framework in $Na_3In_2P_3$ described above has not yet been found in any other phosphidotrielate, but the same structure motif is also observed in several compounds of nitrogen, the lighter homologue of phosphorus ($NaSi_2N_3$,[38] $LiSi_2N_3$,[39] Si_2N_2NH,[40] and Si_2N_2O[41]). The structural relationship is outlined in Figure 4. $NaSi_2N_3$ and $LiSi_2N_3$ show the same framework built from SiN_4 tetrahedra. Si_2N_2NH contains an analogous framework of SiN_3NH tetrahedra, and Si_2N_2O features a similar framework of SiN_3O tetrahedra. All these phases and $Na_3In_2P_3$ crystallize in the same space group $Cmc2_1$ (no. 36). In Table 2 the cell parameters, the *M*–*M* distances (*M*=In, Si) in the six-membered rings and the *M*–*M*–*M* angles in the six-membered rings of $Na_3In_2P_3$, $NaSi_2N_3$, $LiSi_2N_3$, Si_2N_2NH, and Si_2N_2O are listed for comparison. As expected, $Na_3In_2P_3$ has the largest cell volume (732.23(8) Å^3) due to the presence of the elements with the largest ionic radii at all positions, with longer In–P compared to Si–N distances, as well as the highest number of alkali metal cations, whereas the cell volumes of $NaSi_2N_3$, $LiSi_2N_3$, Si_2N_2NH, and Si_2N_2O are very similar in a range between 254.1(3) and 233.4(5) Å^3. In Figure 4 the structural relationship of all five compounds is shown. Obviously, this special structural motif is mainly depending on the relative radii of the framework atoms, i.e. on the favored tetrahedral coordination of the central atoms by suitably sized anions, as well as on the relative 2:3 ratio of the elements, whereas neither the formal charges of the concerning atoms, nor, quite surprisingly, the number or even the presence of counter-cations play a significant role in the formation of the polyanionic structure. The different coordination modes of the alkali metal cations also do not influence the formation of the polyanionic structure. All arrangements can be described as a distorted wurtzite structure, and the phosphorus and nitrogen atoms, respectively, are forming a distorted hexagonal close packing.[39,40] In $Na_3In_2P_3$, all octahedral voids are fully occupied by sodium atoms, and the different NaP_6 octahedra are connected via edges and faces (see Figure 4 on the right). In $NaSi_2N_3$, only one

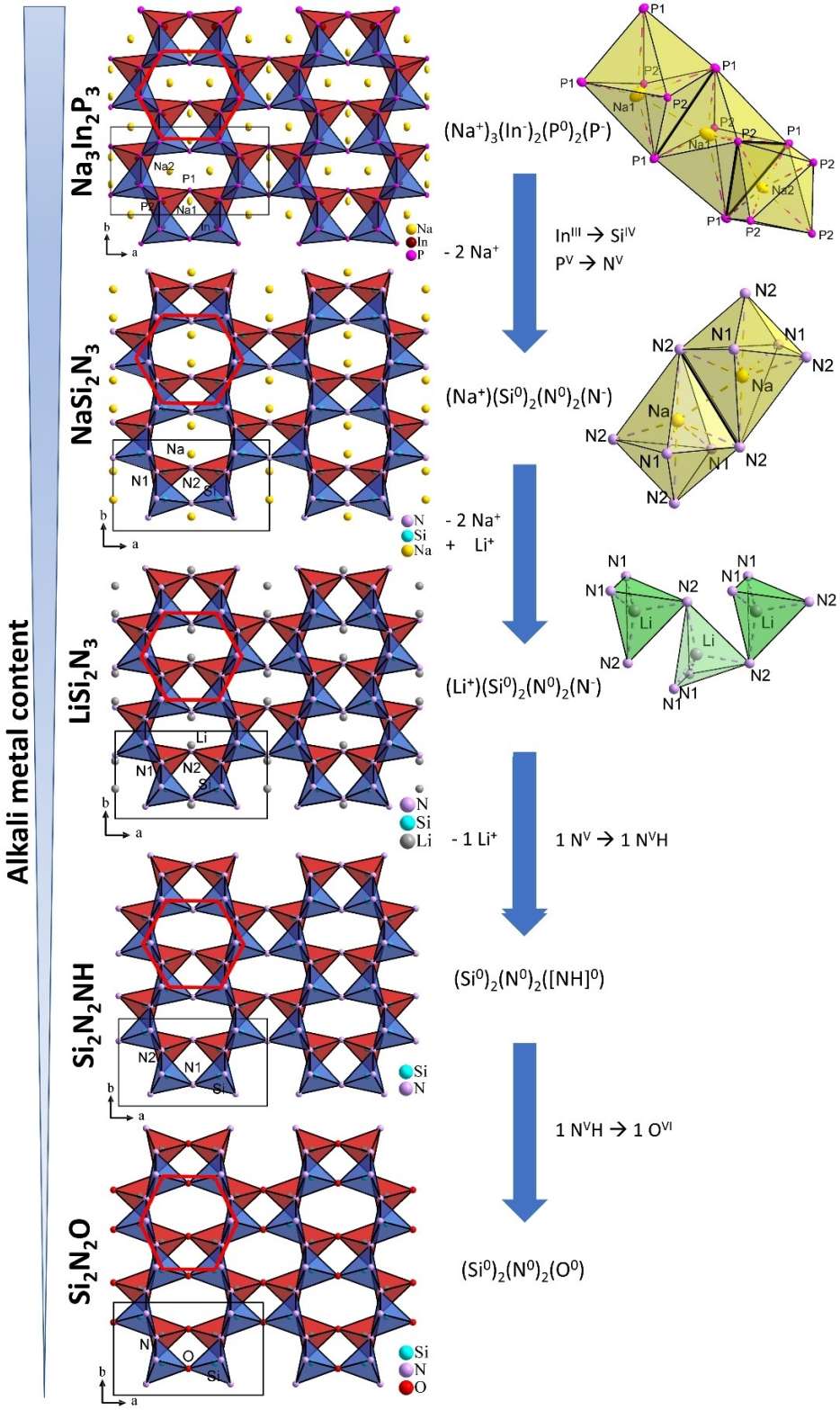

Figure 4. Structural relationship between $Na_3In_2P_3$, $NaSi_2N_3$,[4] $LiSi_2N_3$,[5] Si_2N_2NH,[6] and Si_2ON_2.[7] which exhibit the same connectivity pattern within the framework of corner-sharing tetrahedra. The compounds are ordered from the top with decreasing alkali metal content. Every compound can be written as an electronically balanced formula. The coordination polyhedra of the respective alkali metal are shown on the right. $Na_3In_2P_3$ contains NaP_6 octahedra, which are connected via edges and faces; in $NaSi_2N_3$ the NaP_6 octahedra are connected only via edges, and $LiSi_2N_3$ contains corner-sharing LiP_4 tetrahedra.

third of the octahedral voids is occupied by sodium in a quite distorted fashion (Wyckoff position 4*a*), and the adjacent NaN_6 octahedra are solely connected via edges. In $LiSi_2N_3$, the lithium atoms are placed in one sixth of the tetrahedral voids. The LiN_4

Table 2. Comparison of the cell parameters, and the *M*–*M* distances (*M*=In, Si) of the six-membered rings along the two-fold bonded P and N atoms and along the three-fold bonded P and N atoms, and the *M*–*M*–*M* angles in $Na_3In_2P_3$, $NaSi_2N_3$,[38] $LiSi_2N_3$,[39] Si_2N_2NH,[40] and Si_2ON_2.[41]

	$Na_3In_2P_3$	$NaSi_2N_3$	$LiSi_2N_3$	Si_2N_2NH	Si_2N_2O
	$(Na^+)_3$ $(In^-)_2(P^-)(P^0)_2$	(Na^+) $(Si^0)_2(N^-)(N^0)_2$	(Li^+) $(Si^0)_2(N^-)(N^0)_2$	$(Si^0)([NH]^0)(N^0)_2$	$(Si^0)_2(O^0)(N^0)_2$
a/Å	13.795(1)	9.468(1)	9.2215(9)	9.1930(7)	8.843(5)
b/Å	7.6632(5)	5.502(1)	5.2964(8)	5.4069(4)	5.473(5)
c/Å	6.9266(4)	4.878(5)	4.7798(5)	4.8190(4)	4.835(5)
V/$Å_3$	732.23(8)	254.1(3)	233.4(5)	239.65(3)	234.0(3)
d(*M*–*M*)/Å via 2b–P/N via 3b–P/N	4.5692(3) 4.4835(2)	3.231(9) 3.131(8)	3.060(1) 3.0675(8)	3.194(9) 3.04(1)	3.118(9) 3.031(6)
M–*M*–*M*/°	121.285(1), 117.431(1)	118.5(2), 112.9(2)	120.315(5), 119.37(2)	117.4(2), 125.2(5)	115.5(2), 129.1(1)

tetrahedra are connected via corners to one-dimensional infinite chains.

All compounds show the same network of six-membered rings in graphite-like layers. The edges of the hexagons can be characterized by (non-bonding) *M*–*M* distances (*M*=In, Si). The six-membered rings are slightly distorted, shown by the deviation of the *M*–*M* distances along the two-fold connected P and N atoms and the three-fold connected P and N atoms (Table 2). In most cases the edges of the hexagons via the two-fold bonded (2b) P and N atoms are slightly longer than the edges via the three-fold bonded (3b) P and N atoms. This is also reflected by the deviation of the *M*–*M*–*M* angles of the hexagons compared to the ideal angle of 120°. Only $LiSi_2N_3$ shows almost perfect hexagonal layers, with almost equal Si–Si distances of 3.060 and 3.0675 Å and *M*–*M*–*M* angles (120.315 and 119.37°).

Electronic structures

In all investigated compounds the *Tr* atoms form four covalent bonds to four P atoms. Thus, a formal charge of −1 results for each *Tr* atom. For the occurring two- and three-fold covalently connected P atoms a formal charge of −1 and 0, respectively, can be assigned. Since the alkali metal cations Li and Na possess one positive charge each, all compounds correspond to electronically balanced formulas: $A_3TrP_2 = [(A^+)_3(4b\text{-}Tr^-)(2b\text{-}P^-)_2]$ for A=Li, Na and *Tr*=Al, In, Ga as well as $Na_3In_2P_3$=$[(Na^+)_3(In^-)_2(P^-)(P^0)_2]$.

The electronic band structures of Li_3AlP_2, Li_3GaP_2, Li_3InP_2, Na_3InP_2, and $Na_3In_2P_3$ calculated at the DFT-PBE0/TZVP level of theory are shown in Figure 5 and reveal the semiconducting property anticipated by the formal charge allocation. Band structures are plotted along the lines between the high-symmetry points in the Brillouin Zone (BZ), and the electronic density of states (DOS) are projected on the atoms (partial DOS). The optimized structures of the indium compounds are in line with the experimental crystal structures, since the deviations of the cell parameters and In–P distances are less than 1.2% (Table S7–S9).

In all compounds the valence band maxima (VBMs) and the conduction band minima (CBMs) are both located at the Γ point, disclosing a direct band gap for all compounds with calculated values of 3.1 eV (Li_3AlP_2),[15] 2.8 eV (Li_3GaP_2),[15] 2.7 eV (Li_3InP_2, Figure S17), 2.1 eV (Na_3InP_2, Figure S18), and 2.1 eV ($Na_3In_2P_3$, Figure S16). Interestingly, there are direct band gaps in this compound family despite the different symmetry of the individual structures.

We note also that the conduction bands (CBs) near the CBMs as well as the valence bands (VBs) near the VBMs all show significant dispersion. In addition, the VBs approach the energy values of the VBMs at several other points in all compounds except $Na_3In_2P_3$. This hints for the possibility of multiple optical transitions between band edges including indirect transitions. Although P and *Tr* states appear simultaneously in the CBMs, the CBMs are mostly dominated by states of the triel element as visible from the partial DOS in Figure 5. By comparing all individual Wyckoff positions in the DOS plots of the indium compounds, the phosphorus position contributes almost equally at the Fermi level in Na_3InP_2 and $Na_3In_2P_3$ (Figures S18 and S16). Since the VBs and their maximum originate from P orbitals, and the CBs are dominated by P and triel elements, the interaction of the triel elements and the P atoms determine the size of the band gap.

UV-Vis measurements. The nature and size of the band gaps of the phosphide-based materials Li_3TrP_2 (*Tr*=Al, Ga, In), Na_3InP_2 and $Na_3In_2P_3$ were experimentally determined by solid-state UV-Vis measurements (Figure S19). The Tauc plot analyses (Figure 6)[50] suggest that all compounds are direct band gap semiconductors with decreasing band gaps in the row 2.45 eV (Li_3AlP_2), 2.18 eV (Li_3GaP_2), 1.99 eV (Li_3InP_2), 1.37 eV (Na_3InP_2), and 1.27 eV ($Na_3In_2P_3$). All experimentally determined and calculated band gaps are listed in Table 3. The experimentally observed band gaps of all compounds are 0.62 to 0.73 eV smaller than the calculated ones, which is in line with the well-known tendency that the DFT-PBE0 method overestimates band gaps in this range.[51] Nevertheless, the trend of decreasing band gaps in the series Li_3TrP_2 (*Tr*=Al, Ga, In), Na_3InP_2 and $Na_3In_2P_3$ is fully reproduced.

Table 3. Direct band gaps determined experimentally and by DFT-PBE0 calculations of Li_3AlP_2, Li_3GaP_2, Li_3InP_2, Na_3InP_2, and $Na_3In_2P_3$.

	Li_3AlP_2	Li_3GaP_3	Li_3InP_2	Na_3InP_2	$Na_3In_2P_3$
$E_{g\ exp}$/eV	2.45	2.18	1.99	1.37	1.27
$E_{g\ calc}$/eV	3.1	2.8	2.7	2.1	2.0

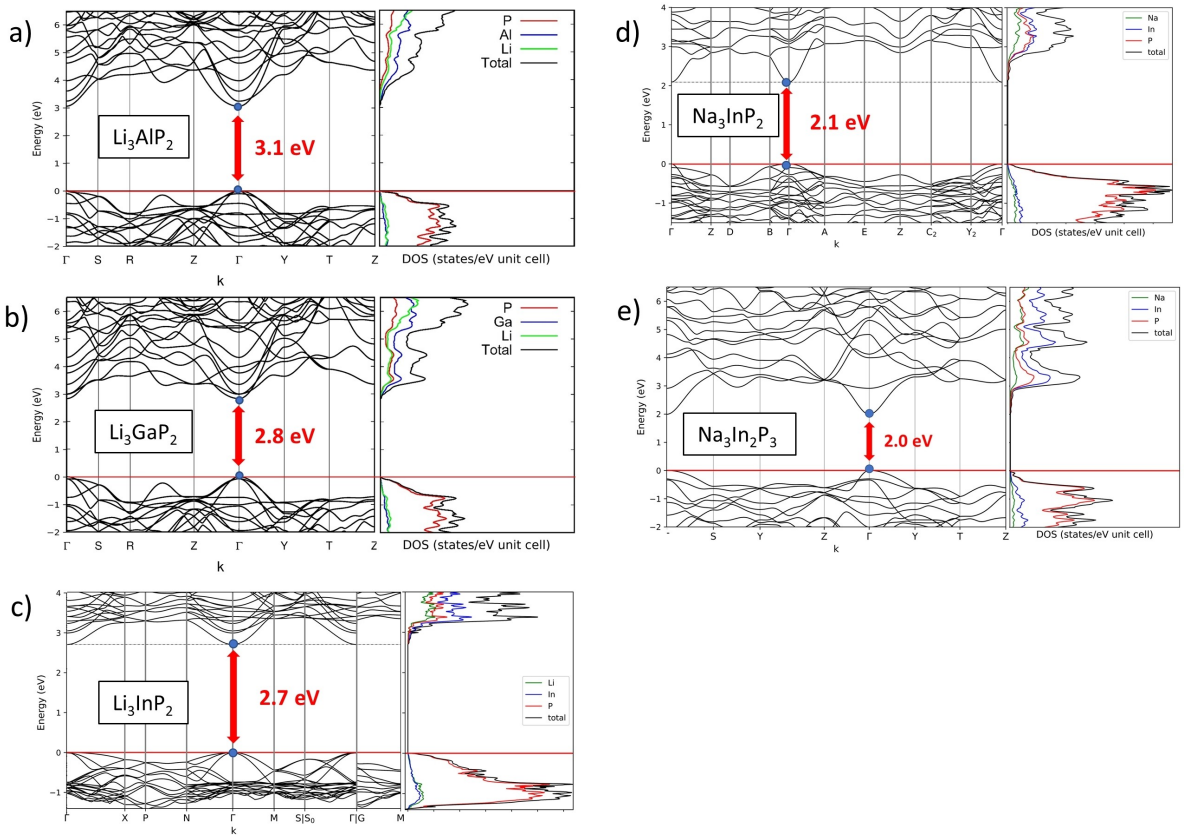

Figure 5. Electronic band structure and density of states (DOS) of Li_3AlP_2 (a), Li_3GaP_2 (b), Li_3InP_2 (c), Na_3InP_2 (d), and $Na_3In_2P_3$ (e) exhibiting direct band gaps (red arrow). Additional optically indirect transitions are indicated by yellow arrows. The Fermi level is set at 0 eV. The band structures of Li_3AlP_2 and Li_3GaP_2 are reprinted and modified with permission from Wiley-VCH Verlag GmbH & Co. KGaA: *Chem. Eur. J.* 2020, *26*, 6812–6819, © 2020. This is an open access article distributed under the terms of the Creative Commons CC BY license.

Conclusions

Direct band gap semiconductors are most promising for applications in optoelectronic applications due to their high efficiency compared to mainly used semiconductors with indirect band gaps. The here investigated lithium and sodium phosphidotrielates can easily be synthesized and show rather distinct VBMs and CBMs with large dispersion. All structures comprise the same building units of TrP_4 tetrahedra that are connected in various ways. Whereas Li_3AlP_2, Li_3GaP_2 and Na_3InP_2 contain edge- and vertex-sharing tetrahedra, Li_3InP_2 and $Na_3In_2P_3$ show exclusively vertex-sharing tetrahedra. With respect to the connectivity, all compounds contain two-fold connected P atoms, however, in $Na_3In_2P_3$ also three-connected P atoms occur. Despite the different symmetries of their crystal structures, all compounds are direct band gap semiconductors. The series of phosphidotrielates spans an exceptionally large range of direct band gaps from 2.45 to 1.27 eV. In the Gibbs composition triangles of each triel element, the compounds are positioned on an imaginary line connecting Li_3P or Na_3P and *Tr*P. Therefore phosphidotrielates hint for a large structural variety, and more different structures can be expected by variation of the Li_3P:*Tr*P or Na_3P:*Tr*P ratio. Besides the ratio of alkali metal to TrP_4 units, also the nature of the alkali metal is responsible for the connectivity of the polyanions, and larger cations induce lower dimensionalities of the anionic partial structures. For example, the substitution with the larger potassium ions lead to a segregation of the 3D polyanionic framework in Na_3InP_2 into chains of edge-sharing InP_4 tetrahedra in K_3InP_2.[52] Furthermore, the heavier homologues Rb_3InP_2 and Cs_3InP_2 exhibit twisted InP_4 chains and even dimers of InP_3 triangles.[53–54] All these compounds could exhibit interesting semiconducting properties and are in the focus of future investigations.

According to the quantum chemical calculations, the size of the band gap for such materials might be determined by the *Tr*–P interactions, which might trigger further studies within this field.

Experimental Section

All steps of synthesis and sample preparation were carried out inside an argon-filled glove box (Mbraun, $p(H_2O)$, $p(O_2) < 0.1$ ppm). Prior to use, sodium (Na, rods, Merck-Schuchardt, >99%) was cleaned from oxide layers. Indium (In, drops, Sigma-Aldrich, 99.9%) and phosphorus (P, powder, Sigma-Aldrich, 97%) were used without any further purification. Li_3AlP_2, Li_3GaP_2 and Li_3InP_2 were synthesised according to literature (see Figures S5, S6 and S7).[15,18]

Synthesis of $Na_3In_2P_3$. $Na_3In_2P_3$ was synthesized from the elements *via* ball milling and subsequent annealing. Sodium (540.1 mg, 23.26 mmol, 3.0 equiv.), indium (1782.0 mg, 15.50 mmol, 2.0 equiv.), and phosphorus (742.6 mg, 23.26 mmol, 3.0 equiv.) were ball milled (Fritsch Pulverisette 6) 72 times at 350 rpm with resting periods (every 10 min for 5 min) using a WC milling set (45 mL jar and with 7 balls with a diameter of 1.5 cm) resulting in a reactive mixture which according to

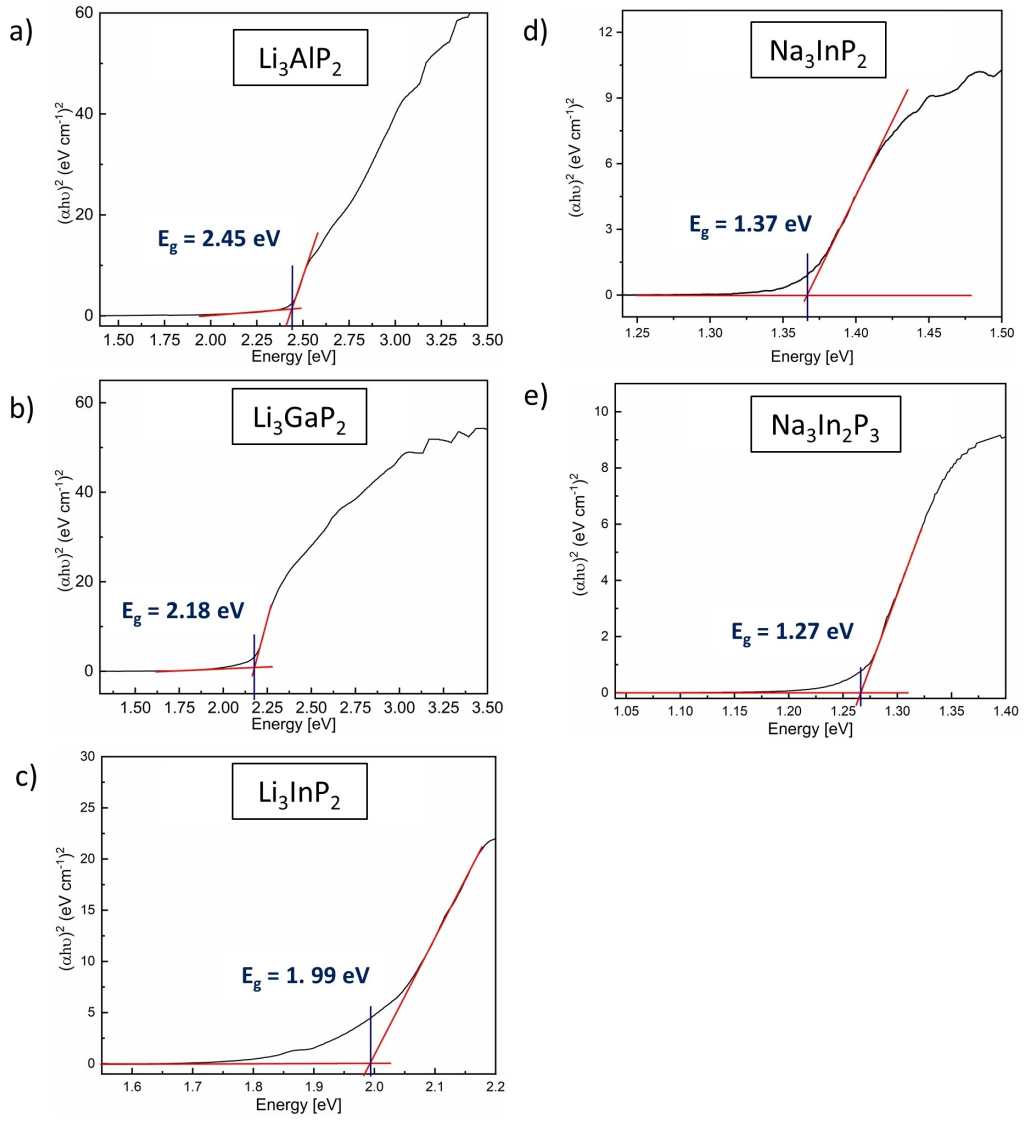

Figure 6. Tauc plots of a) Li_3AlP_2, b) Li_3GaP_2, c) Li_3InP_2, d) Na_3InP_2, and e) $Na_3In_2P_3$ obtained from solid-state UV-vis measurements (see Figure S19). The compounds are direct band gap semiconductors with band gaps of 1.27 eV for $Na_3In_2P_3$, 1.37 eV for Na_3InP_2, 1.99 eV for Li_3InP_2, 2.18 eV for Li_3GaP_2, and 2.45 eV for Li_3AlP_2.

the powder X-ray diffractogram contained small amounts of crystalline material of the title compound, unreacted indium and Na_3P (Figure S2). The black mixture was pressed into pellets with a diameter of 13 mm for 30 s at 5 t using a hydraulic press (Specac Atlas 15T). The fragmented pellets were filled into a niobium ampoule (8 mm diameter). The ampoule was sealed in an electric arc furnace (Edmund Bühler MAM1), enclosed in a silica reaction container under vacuum and subsequently heated with 5 $K \cdot min^{-1}$ up to 673 K and dwelled for 48 h in a tube furnace (HTM Reetz Loba 1200–42-600-1-OW with a EUROTHERM S 14083 temperature controller). Afterwards the pellets were ground, and the annealing procedure was repeated at 773 K for 96 h yielding black, microcrystalline $Na_3In_2P_3$ with small amounts of Na_3InP_2 and InP as by-products (Figure 1). The $Na_3In_2P_3$: Na_3InP_2 : InP ratio is 97.0(1) : 1.8(1) : 1.2(1) wt.–% as determined by Rietveld refinement. For the characterization of $Na_3In_2P_3$ by differential scanning calorimetry and impedance spectroscopy see Supporting Information.

Grey single crystals were obtained by the reaction of sodium, indium and phosphorus with the formal stoichiometry "$Na_3In_4P_5$" in a tantalum ampoule. Sodium (31.0 mg, 1.35 mmol, 3.0 equiv.), indium (204.3 mg, 1.78 mmol, 4.0 equiv.) and phosphorus (71.0 mg, 2.29 mmol, 5.1 equiv.) were filled into a tantalum ampoule. The ampoule was sealed in an electric arc furnace (Edmund Bühler MAM1), enclosed in a silica reaction container under vacuum and subsequently heated with 5 $K \cdot min^{-1}$ up to 1073 K, dwelled for 24 h and cooled with 0.5 $K \cdot min^{-1}$ to room temperature in a tube furnace (HTM Reetz Loba 1200–42-600-1-OW with a EUROTHERM S 14083 temperature controller), yielding a metallic to black product. Besides $Na_3In_2P_3$, the product contains Na_3InP_2 and InP according to the powder X-ray diffraction pattern (Figure S2). Details of the structure refinement of $Na_3In_2P_3$ from single crystal X-ray diffraction data are listed in Table S3 and further data are given in Tables S3–S6 in the Supporting Information.

Synthesis of Na_3InP_2: Na_3InP_2 was synthesized from the elements *via* ball milling and subsequent annealing. Sodium (848.1 mg, 36.52 mmol, 3.0 equiv.), indium (1399.2 mg, 12.17 mmol, 1.0 equiv.) and phosphorus (777.5 mg, 24.35 mmol, 2.0 equiv.) were ball milled (Fritsch Pulverisette 6) 72 times at 350 rpm with resting periods (every 10 min for 5 min) using a WC milling set (45 mL jar and with 7 balls with a diameter of 1.5 cm). The black mixture was pressed into pellets with a diameter of

13 mm for 30 s at 5 t using a hydraulic press (Specac Atlas 15T). The fragmented pellets were filled into a niobium ampoule (8 mm diameter). The ampoule was sealed in an electric arc furnace (Edmund Bühler MAM1), enclosed in a silica reaction container under vacuum and subsequently heated with 5 K·min^{-1} up to 673 K and dwelled for 48 h in a tube furnace (HTM Reetz Loba 1200–42-600-1-OW with a EUROTHERM S 14083 temperature controller). After grinding, a moisture and air sensitive black powder was obtained. Besides Na_3InP_2, the sample showed only a few unknown reflections with low intensity (Figure S3).

Powder X-ray diffraction. For powder X-ray diffraction (PXRD) measurements, the samples were ground in an agate mortar and sealed inside 0.3 mm glass capillaries. PXRD measurements were performed at room temperature on a Stadi P diffractometer (Stoe & Cie) equipped with a Ge(111) monochromator for Cu $K_{\alpha1}$ radiation ($\lambda = 1.54056$ Å) or Mo $K_{\alpha1}$ radiation ($\lambda = 0.7093$ Å) and a MYTHEN DCS 1 K (Dectris) solid-state detector. The raw powder data were processed with the software package WinXPOW.[55]

Rietveld refinement. Rietveld refinements were performed with TOPAS V6.[56] The data of the single crystal structure determination were used as the structural model. All cell parameters, atom positions and isotropic displacement parameters were refined freely.

Single crystal structure determination. A single crystal of $Na_3In_2P_3$ was sealed in a 0.3 mm glass capillary. The single crystal X-ray diffraction measurement was performed on a Stadivari diffractometer (Stoe & Cie) equipped with a Ge(111) monochromator, an Mo K_α radiation ($\lambda =$ 0.71073 Å) source and a PILATUS 3R 300 K detector (Dectris). The structure was solved by Direct Methods (SHELXS) and refined by full-matrix least-squares calculations against F^2 (SHELXL).[57] Deposition Number 2002756 (for $Na_3In_2P_3$) contains the supplementary crystallographic data for this paper. These data are provided free of charge by the joint Cambridge Crystallographic Data Centre and Fachinformationszentrum Karlsruhe Access Structures service.

NMR spectroscopy. Magic angle spinning (MAS) NMR spectroscopy was carried out on a Bruker Avance 300 NMR device operating at 7.04 T by the use of a 4 mm ZrO_2 rotor. The resonance frequencies of the measured nucleus ^{31}P was 121.46 MHz. The rotational frequency was 15 kHz. The MAS spectrum was obtained at room temperature with relaxation delays of 30 s and 1440 scans. The ^{31}P spectrum is referred to ammonium dihydrogen phosphate (s) with a chemical shift of 1.11 ppm with reference to concentrated H_3PO_4. The spectrum was recorded using single-pulse excitation. The ^{31}P MAS-NMR spectrum of $Na_3In_2P_3$ shows one very broad, asymmetric signal between −80 and −200 ppm (Figure S10), and thus, the two crystallographically different phosphorus positions cannot be distinguished. The observed range of signals, however, corresponds to the chemical shift regime of three-bonded P^0 such as in $Li_3Si_3P_7$ (−77.4 and −121.1 ppm) and two-bonded P^{-1} like in $Li_3Si_3P_7$ (−168.8 and −178.7 ppm) and Li_2SiP_2 (−129.1 and −241.5 ppm).[13,16]

Electronic structure calculations. The computational studies of Li_3InP_2, Na_3InP_2, and $Na_3In_2P_3$ were performed using the CRYSTAL17 program package and hybrid density functional methods.[58–59] A hybrid exchange-correlation functional after Perdew, Burke and Ernzerhof (DFT-PBE0) was used.[60–61] Localized, Gaussian-type triple-ζ-valence + polarization level basis sets were used for In and P and split valence + polarization level basis sets for Li and Na. The basis sets were derived from the molecular Karlsruhe basis sets (further basis set details are given in the Supporting Information).[62–65] For the evaluation of the Coulomb and exchange integrals (TOLINTEG), tight tolerance factors of 8, 8, 8, 8, 16 were used for all calculations. The reciprocal space of Li_3InP_2, Na_3InP_2 and $Na_3In_2P_3$ were sampled with 3×3×3, 4×5×2, and 5×5×5 Monkhorst-Pack-type *k*-point grids, respectively.[66] The starting geometries were taken from the experimental data, and both the lattice parameters and atomic positions were fully optimized within the constraints imposed by the space group symmetry. The optimized structures were confirmed to be true local minima by means of harmonic frequency calculations at the Γ-point[67–68] (no imaginary frequencies). Electronic band structures and density of states (DOS) were calculated. The Brillouin Zone path of $Na_3In_2P_3$, Γ–S–Y–Z–Γ–Y–T–Z, is derived from the paths of Setyawan and Curtarolo.[69] All other Brillouin Zone paths were provided by the web service *SeeK-path*.[70]

UV-vis measurements. Solid-state UV-vis spectra were recorded on a *Shimadzu* UV-3600 Plus UV-vis-NIR spectrophotometer. Powder samples were fixed between two quartz slides under Ar atmosphere and sealed with vacuum grease for the measurement. In case of $Na_3In_2P_3$, Na_3InP_2 and Li_3InP_2, the powder samples were mixed with $BaSO_4$, and in case of Li_3AlP_2 and Li_3GaP_2, the pure powders were used. Measurement parameters: medium scan speed, slit width (20) with external (3Detector) unit, enabled stair correction, baseline correction ($BaSO_4$ background) S/R exchange normal, slit and detector lock normal. Additionally, a light source change at 287 nm, detector change at 870 nm, and grating change at 700 nm were applied, causing minor absorption changes at these wavelengths. Direct band gaps were calculated from the material absorption *A* in the respective solid-state UV-vis spectrum following literature methods.[50] Applied formula:

$$E\ (\mathrm{eV}) = \frac{1240}{\lambda\ (\mathrm{nm})}$$

$$(\alpha h\upsilon)^2 = (2.303 \cdot E \cdot A)^2$$

Supporting Information

Experimental powder X-ray diffraction patterns, results of the Rietveld analysis, details of the single crystal structure determination, Gibbs composition triangle of Na–In–P, comparison of $Na_3In_2P_2$ with sepiolite, differential scanning calorimetry (DSC), ^{31}P MAS-NMR spectrum, electrochemical characterization, results of the quantum chemical calculations, solid-state UV-vis measurements

Acknowledgements

We thank the Bavarian State Ministry for Education, Science and Arts within the project "SolarTechnologies go Hybrid" and the Bavarian Ministry of Economic Affairs, Regional Development and Energy within the project "Industrialisierbarkeit von Festkörperelektrolytzellen" for funding. Open Access funding enabled and organized by Projekt DEAL.

Conflict of Interests

The authors declare no conflict of interest.

Data Availability Statement

The data that support the findings of this study are available in the supplementary material of this article.

Keywords: crystal structure · direct band gap · indium · phosphide · semiconductor

[1] J. Mark, M. P. Hanrahan, K. E. Woo, S. Lee, A. J. Rossini, K. Kovnir, *Chem. Eur. J.* **2019**, *25*, 6392–6401.
[2] W. Wang, J. Zhang, D. Y. W. Yu, Q. Li, *J. Power Sources* **2017**, *364*, 420–425.
[3] S. Liu, H. Zhang, L. Xu, L. Ma, X. Chen, *J. Power Sources* **2016**, *304*, 346–353.
[4] K.-W. Tseng, S.-B. Huang, W.-C. Chang, H.-Y. Tuan, *Chem. Mater.* **2018**, *30*, 4440–4447.
[5] Y. Kim, Y. Kim, A. Choi, S. Woo, D. Mok, N.-S. Choi, Y. S. Jung, J. H. Ryu, S. M. Oh, K. T. Lee, *Adv. Mater.* **2014**, *26*, 4139–4144.
[6] G. Coquil, B. Fraisse, N. Dupré, L. Monconduit, *ACS Appl. Energ. Mater.* **2018**, *1*, 3778–3789.
[7] S. Strangmüller, H. Eickhoff, D. Müller, W. Klein, G. Raudaschl-Sieber, H. Kirchhain, C. Sedlmeier, V. Baran, A. Senyshyn, V. L. Deringer, L. van Wüllen, H. A. Gasteiger, T. F. Fässler, *J. Am. Chem. Soc.* **2019**, *141*, 14200–14209.
[8] H. Eickhoff, S. Strangmüller, W. Klein, H. Kirchhain, C. Dietrich, W. G. Zeier, L. van Wüllen, T. F. Fässler, *Chem. Mater.* **2018**, *30*, 6440–6448.
[9] S. Strangmüller, H. Eickhoff, G. Raudaschl-Sieber, H. Kirchhain, C. Sedlmeier, L. van Wüllen, H. A. Gasteiger, T. F. Fässler, *Chem. Mater.* **2020**, *32*, 6925–6934.
[10] T. M. F. Restle, C. Sedlmeier, H. Kirchhain, W. Klein, G. Raudaschl-Sieber, V. L. Deringer, L. van Wüllen, H. A. Gasteiger, T. F. Fässler, *Angew. Chem. Int. Ed.* **2020**, *59*, 5665–5674.
[11] T. M. F. Restle, C. Sedlmeier, H. Kirchhain, W. Klein, G. Raudaschl-Sieber, L. van Wüllen, T. F. Fässler, *Chem. Mater.* **2021**, *33*, 2957–2966.
[12] S. Strangmüller, H. Eickhoff, W. Klein, G. Raudaschl-Sieber, H. Kirchhain, T. Kutsch, V. Baran, A. Senyshyn, L. van Wüllen, H. A. Gasteiger, T. F. Fässler, *J. Mater. Chem. A* **2021**, *9*, 15254–15268.
[13] H. Eickhoff, L. Toffoletti, W. Klein, G. Raudaschl-Sieber, T. F. Fässler, *Inorg. Chem.* **2017**, *56*, 6688–6694.
[14] H. Eickhoff, C. Sedlmeier, W. Klein, G. Raudaschl-Sieber, H. A. Gasteiger, T. F. Fässler, *Z. Anorg. Allg. Chem.* **2020**, *646*, 95–102.
[15] T. M. F. Restle, J. V. Dums, G. Raudaschl-Sieber, T. F. Fässler, *Chem. Eur. J.* **2020**, *26*, 6812–6819.
[16] L. Toffoletti, H. Kirchhain, J. Landesfeind, W. Klein, L. van Wüllen, H. A. Gasteiger, T. F. Fässler, *Chem. Eur. J.* **2016**, *22*, 17635–17645.
[17] A. Haffner, T. Bräuniger, D. Johrendt, *Angew. Chem.* **2016**, *128*, 13783–13786.
[18] T. M. F. Restle, V. L. Deringer, J. Meyer, G. Raudaschl-Sieber, T. F. Fässler, *Chem. Sci.* **2021**, *12*, 1278–1285.
[19] S. Kasap, C. Koughia, P. Capper, *Springer Handbook of Electronic and Photonic Materials* Springer, **2006**, 54.
[20] L. Venema, *Nature* **2011**, *479*, 309–309.
[21] A. Amon, E. Svanidze, A. Ormeci, M. König, D. Kasinathan, D. Takegami, Y. Prots, Y.-F. Liao, K.-D. Tsuei, L. H. Tjeng, A. Leithe-Jasper, Y. Grin, *Angew. Chem. Int. Ed.* **2019**, *58*, 15928–15933.
[22] D. E. Aspnes, A. A. Studna, *Phys. Rev. B* **1983**, *27*, 985–1009.
[23] R. Soref, B. Bennett, *IEEE J. Quantum Electron.* **1987**, *23*, 123–129.
[24] M. Razeghi, *Nature* **1994**, *369*, 631–633.
[25] K. Zhang, L. Guo, *Catal. Sci. Technol.* **2013**, *3*, 1672–1690.
[26] T. K. Bera, J.-H. Song, A. J. Freeman, J. I. Jang, J. B. Ketterson, M. G. Kanatzidis, *Angew. Chem. Int. Ed.* **2008**, *47*, 7828–7832.
[27] E. C. Agha, C. D. Malliakas, J. Im, H. Jin, L.-D. Zhao, A. J. Freeman, M. G. Kanatzidis, *Inorg. Chem.* **2014**, *53*, 673–675.
[28] J. Zhao, S. M. Islam, O. Y. Kontsevoi, G. Tan, C. C. Stoumpos, H. Chen, R. K. Li, M. G. Kanatzidis, *J. Am. Chem. Soc.* **2017**, *139*, 6978–6987.
[29] Y. Petroff, M. Balkanski, J. P. Walter, M. L. Cohen, *Solid State Commun.* **1969**, *7*, 459–462.
[30] T. K. Bera, J. I. Jang, J.-H. Song, C. D. Malliakas, A. J. Freeman, J. B. Ketterson, M. G. Kanatzidis, *J. Am. Chem. Soc.* **2010**, *132*, 3484–3495.
[31] K. E. Woo, J. Wang, K. Wu, K. Lee, J.-A. Dolyniuk, S. Pan, K. Kovnir, *Adv. Funct. Mater.* **2018**, *28*, 1801589.
[32] J. Mark, J. Wang, K. Wu, J. G. Lo, S. Lee, K. Kovnir, *J. Am. Chem. Soc.* **2019**, *141*, 11976–11983.
[33] J. Mark, J.-A. Dolyniuk, N. Tran, K. Kovnir, *Z. Anorg. Allg. Chem.* **2019**, *645*, 242–247.
[34] T. Yu, S. Wang, X. Zhang, C. Li, J. Qiao, N. Jia, B. Han, S.-Q. Xia, X. Tao, *Chem. Mater.* **2019**, *31*, 2010–2018.
[35] S. Lee, S. L. Carnahan, G. Akopov, P. Yox, L.-L. Wang, A. J. Rossini, K. Wu, K. Kovnir, *Adv. Funct. Mater.* **2021**, *31*, 2010293.
[36] W. Blase, G. Cordier, M. Somer, *Z. Kristallogr.* **1991**, *195*, 119–120.
[37] K. Brauner, A. Preisinger, *Tschermaks Mineral. Petrogr. Mitt.* **1956**, *6*, 120–140.
[38] H. Jacobs, H. Mengis, *Eur. J. Solid State Inorg. Chem.* **1993**, *30*, 45–53.
[39] M. Orth, W. Schnick, *Z. Anorg. Allg. Chem.* **1999**, *625*, 1426–1428.
[40] D. Peters, H. Jacobs, *J. Less-Common Met.* **1989**, *146*, 241–249.
[41] I. Idrestedt, C. Brosset, *Acta Chem. Scand.* **1964**, *18*, 1879–1886.
[42] G. Cordier, H. Schäfer, M. Steher, *Z. Naturforsch. B* **1985**, *40*, 1100–1104.
[43] G. Cordier, H. Schäfer, M. Stelter, *Z. Naturforsch. B* **1986**, *41*, 1416–1419.
[44] M. Somer, W. Carrillo-Cabrera, K. Peters, H. G. V. Schnering, *Z. Kristallogr. New Cryst. Struct.* **1998**, *213*, 4–4.
[45] G. Cordier, H. Schäfer, M. Stelter, *Z. Naturforsch. B* **1987**, *42*, 1268–1272.
[46] W. Carrillo-Cabrera, M. Somer, K. Peters, H. G. von Schnering, *Chem. Ber.* **1996**, *129*, 1015–1023.
[47] A. Addamiano, *J. Am. Chem. Soc.* **1960**, *82*, 1537–1540.
[48] H. Eickhoff, C. Dietrich, W. Klein, W. G. Zeier, T. F. Fässler, *Z. Anorg. Allg. Chem.* **2021**, *647*, 28–33.
[49] M. Somer, W. Carrillo-Cabrera, E. M. Peters, H. G. V. Schnering, *Z. Kristallogr.* **1995**, *210*, 777–777.
[50] J. Tauc, R. Grigorovici, A. Vancu, *Phys. Stat. Sol.* **1966**, *15*, 627–637.
[51] B. Civalleri, D. Presti, R. Dovesi, A. Savin, *Chem. Modell.* **2012**, *9*, 168–185.
[52] W. Blase, G. Cordier, *Z. Kristallogr.* **1991**, *195*, 109–110.
[53] M. Somer, W. Carrillo-Cabrera, E. M. Peters, K. Peters, H. G. V. Schnering, *Z. Kristallogr. New Cryst. Struct.* **1998**, *213*, 5–6.
[54] W. Blase, G. Cordier, M. Somer, *Z. Kristallogr.* **1991**, *195*, 123–124.
[55] *WinXPOW*, 3.0.2.1, STOE & Cie GmbH, Darmstadt, Germany, **2011**.
[56] *TOPAS*, 6, Bruker AXS, **2016**.
[57] G. Sheldrick, *Acta Crystallogr. Sect. C. Struct. Chem.* **2015**, *71*, 3–8.
[58] R. Dovesi, V. R. Saunders, C. Roetti, R. Orlando, C. M. Zicovich-Wilson, F. Pascale, B. Civalleri, K. Doll, N. M. Harrison, I. J. Bush, P. D'Arco, M. Llunell, M. Causà, Y. Noël, L. Maschio, A. Erba, M. Rerat, S. Casassa, *CRYSTAL17 User's Manual* University of Torino, **2017**.
[59] R. Dovesi, A. Erba, R. Orlando, C. M. Zicovich-Wilson, B. Civalleri, L. Maschio, M. Rerat, S. Casassa, J. Baima, S. Salustro, B. Kirtman, *WIREs Comput. Mol. Sci.* **2018**, *8*, e1360.
[60] J. P. Perdew, K. Burke, M. Ernzerhof, *Phys. Rev. Lett.* **1996**, *77*, 3865–3868.
[61] C. Adamo, V. Barone, *J. Chem. Phys.* **1999**, *110*, 6158–6170.
[62] G. Sansone, L. Maschio, D. Usvyat, M. Schütz, A. Karttunen, *J. Phys. Chem. Lett.* **2016**, *7*, 131–136.
[63] R. E. Stene, B. Scheibe, A. J. Karttunen, W. Petry, F. Kraus, *Eur. J. Inorg. Chem.* **2019**, *2019*, 3672–3682.
[64] F. Weigend, M. Häser, H. Patzelt, R. Ahlrichs, *Chem. Phys. Lett.* **1998**, *294*, 143–152.
[65] F. Weigend, R. Ahlrichs, *Phys. Chem. Chem. Phys.* **2005**, *7*, 3297–3305.
[66] H. J. Monkhorst, J. D. Pack, *Phys. Rev. B* **1976**, *13*, 5188–5192.
[67] F. Pascale, C. M. Zicovich-Wilson, F. L. Gejo, B. Civalleri, R. Orlando, R. Dovesi, *J. Comput. Chem.* **2004**, *25*, 888–897.
[68] C. M. Zicovich-Wilson, F. Pascale, C. Roetti, V. R. Saunders, R. Orlando, R. Dovesi, *J. Comput. Chem.* **2004**, *25*, 1873–1881.
[69] W. Setyawan, S. Curtarolo, *Comput. Mater. Sci.* **2010**, *49*, 229–321.
[70] Y. Hinuma, G. Pizzi, Y. Kumagai, F. Oba, I. Tanaka, *Comput. Mater. Sci.* **2017**, *128*, 140–184.

Manuscript received: December 18, 2023
Accepted manuscript online: December 31, 2023
Version of record online: February 7, 2024